Advances in Nano Research, *Vol. 13, No.4 (2022) 313-323*
https://doi.org/10.12989/anr.2022.13.4.313

Microstructure characterization and mechanical properties of Cr–Ni/ZrO_2 nanocomposites

Özlem Sevinç[1] and Ege A. Diler*[2]

[1]*Interdisciplinary Division of Materials Science and Engineering, Ege University, 35040, Izmir, Turkey*
[2]*Department of Mechanical Engineering, Ege University, 35040, Izmir, Turkey*

(*Received August 17, 2020, Revised July 18, 2022, Accepted July 29, 2022*)

Abstract. The microstructure and mechanical properties of Cr-Ni steel and Cr-Ni steel-matrix nanocomposites reinforced with nano-ZrO_2 particles were investigated in this study. Cr-Ni steel and Cr-Ni/ZrO_2 nanocomposites were produced using a combination of high-energy ball milling, pressing, and sintering processes. The microstructures of the specimens were analyzed using EDX and XRD. Compression and hardness tests were performed to determine the mechanical properties of the specimens. Nano-ZrO_2 particles were effective in preventing chrome carbide precipitate at the grain boundaries. While t–ZrO_2 was detected in Cr-Ni/ZrO_2 nanocomposites, m–ZrO_2 could not be found. Few α'–martensite and deformation bands were formed in the microstructures of Cr-Ni/ZrO_2 nanocomposites. Although nano-ZrO_2 particles had a negligible impact on the strength improvement provided by deformation-induced plasticity mechanisms in Cr-Ni/ZrO_2 nanocomposites, the mechanical properties of Cr-Ni steel were significantly improved by using nano-ZrO_2 particles. The hardness and compressive strength of Cr-Ni/ZrO_2 nanocomposite were higher than those of Cr-Ni steel and enhanced as the weight fraction of nano-ZrO_2 particles increased. Cr-Ni/ZrO_2 nanocomposite with 5wt.% nano-ZrO_2 particles had almost twofold the hardness and compressive strength of Cr-Ni steel. The nano-ZrO_2 particles were considerably more effective on particle-strengthening mechanisms than deformation-induced strengthening mechanisms in Cr-Ni/ZrO_2 nanocomposites.

Keywords: Cr-Ni steel; deformation-induced strengthening mechanisms; nanocomposite; nano-ZrO_2

1. Introduction

High-alloyed austenitic stainless steels are continuously being developed to meet the demands for superior properties in automotive applications, such as high energy absorption and strength (Weidner *et al*. 2020).

The ductility of steel diminishes as its strength increases. Transformation- and twinning-induced plasticity (TRIP/TWIP) steels, on the other hand, provide an outstanding balance of strength and ductility (Biermann and Anerizis *et al*. 2020). These properties can be obtained by deformation-induced phase transformations and mechanical twinning mechanisms that occur during the deformation of TRIP/TWIP steels (El-Sherbiny *et al*. 2020, Opiela *et al*. 2020). The TRIP effect in steels causes the metastable austenite phase (γ) to transform into ε-martensite (hexagonal close-packed) and α'-martensite (bulk-centered cubic) due to the strain-induced transformation mechanisms during the deformation process (Song *et al*. 2019, Järvenpää *et al*. 2020).

The mechanical properties of TRIP/TWIP steels can be improved further by reinforcing with ceramic particles due to the particle-strengthening mechanisms (Hall-Petch-Zener, Orowan, etc.). When TRIP-steel composites are reinforced with ZrO_2 particles, the transformation-induced strengthening provided by ZrO_2 particles can contribute even more to improving mechanical properties (Eckner *et al*. 2016). Almost all studies on TRIP steel matrix composites used micro-sized reinforcement particles to improve the mechanical properties of TRIP steels (Martin *et al*. 2011, 2013, Glage *et al*. 2013, Prüger *et al*. 2013, Weigelt *et al*. 2015, Eckner *et al*. 2016, Weigelt *et al*. 2017, Kirschner *et al*. 2021). On the other hand, there have been very few studies on TRIP steels reinforced with nanoparticles. Nano-sized reinforcement particles have a much greater influence on strengthening mechanisms that improve the mechanical properties of metal matrix composites than micro-sized particles due to the following mechanisms (Casati and Vedani 2014, Malaki *et al*. 2019): The increase in dislocation density induced by mismatches in the thermal expansion coefficient or elastic modulus between the matrix and the particle leads to dislocation-based strengthening in particle-reinforced composites. This mechanism becomes more effective as the specific surface area of the particle increases. Nanoparticles have larger specific surface area than that of microparticles. Therefore, nanoparticles contribute more to dislocation-based strengthening (Zhao *et al*. 2022). Furthermore, Orowan and Hall-Petch mechanisms are more effective in strengthening nanoparticle-reinforced composites than they do on microparticle-reinforced composites (Bhoi *et al*. 2020). Due to the stronger effect of nano-sized reinforcement particles on the strengthening mechanisms, the mechanical properties of TRIP steels can be improved even further. However, the high agglomeration tendency of nanoparticles may have a negative influence on the mechanical properties of TRIP steels and make their manufacturing difficult. This challenge

*Corresponding author, Assistant Professor, Ph.D.,
E-mail: ege.anil.diler@ege.edu.tr

ISSN: 2287-237X (Print), 2287-2388 (Online)

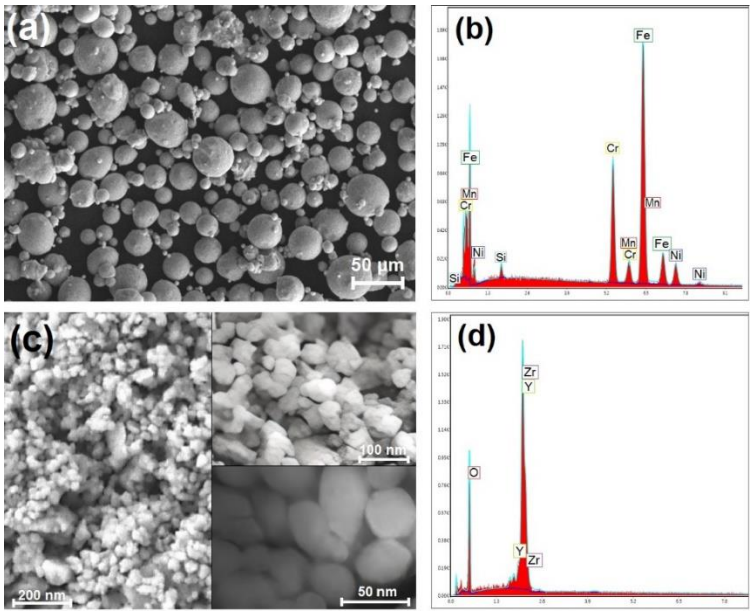

Fig. 1 SEM images of (a) Cr-Ni steel powders and (c) Y_2O_3-stabilized nano-ZrO_2 particles, and XRD analyses of (b) Cr-Ni steel powders and (d) Y_2O_3-stabilized nano-ZrO_2 particles

Table 1 Chemical composition (wt.%) of Cr-Ni steel powder

Cr	Ni	Mn	C	P	S	Si	Fe
17.85	7.1	1.21	0.03	0.045	0.03	1.06	72.68

is largely overcome by using a high-energy ball milling process in the production of metal matrix composites (Alam *et al*. 2022). Nanoparticle-reinforced TRIP steels with superior mechanical properties than microparticle-reinforced TRIP steels can be developed by including high-energy ball milling into the manufacturing process. It should also be noted that the cost of nanoparticles has recently reduced to that of microparticles. For all of these reasons, nanoparticle-reinforced TRIP steels have a strong potential in TRIP steel applications.

For all of these reasons, the goal of this study was to improve the mechanical properties of Cr-Ni steel by reinforcing it with nano-ZrO_2 particles. Cr-Ni/ZrO_2 nano-composites were produced using a combination of high-energy ball milling, pressing, and sintering processes. The effects of nano-ZrO_2 particles on the microstructure and mechanical properties of Cr-Ni steel-based nanocomposites were investigated.

2. Experimental materials and methods

Cr-Ni stainless steel powders were used as the matrix in Cr-Ni/ZrO_2 nanocomposites. The austenitic and metastable high-alloyed Cr-Ni steel matrix powders were spherical in shape and 25±14 µm in average size, as seen in Fig. 1(a), and their chemical composition is given in Table 1 and Fig. 1(b). The nano-sized (40±12 nm) ZrO_2 particles were used as reinforcement element to produce Cr-Ni/ZrO_2 nano-composite as seen in Figs. 1(c) and (d). To stabilize the crystal structure of ZrO_2 particles at room temperature, yttria (Y_2O_3)-stabilized ZrO_2 reinforcement particles were used.

Nano-sized particles have a higher tendency to agglomerate in a metal matrix than microparticles, and particle aggregates have a negative effect on the mechanical properties of particle-reinforced metal matrix composites. Therefore, in order to achieve good (desired) mechanical properties, the optimal number (amount) of reinforcement particles in nanoparticle-reinforced composites is lower than in microparticle-reinforced composites. Although nanocomposites can be reinforced with a lower amount of particles than micro-reinforced composites, they offer better mechanical properties. Therefore, in this study, TRIP steel was reinforced with nano-ZrO_2 particles at lower ratios (1, 2, 3, 4, and 5 wt.%) than that in the micro-ZrO_2 particle-reinforced composites studied in the literature.

Cr-Ni/ZrO_2 nanocomposites were produced using cold pressing and sintering processes combined with high-energy ball milling. Prior to pressing process, Cr-Ni steel powders were reinforced with nano-ZrO_2 reinforcement particles at 1, 2, 3, 4, and 5 wt.% using the high-energy ball milling (mechanical milling) process. In this process, Cr-Ni steel powders, nano-ZrO_2 particles at various weight fractions (1−5 wt.%), and stearic acid (2 wt.%) were mixed and milled for 12 hours in stainless steel jars with chromium steel balls (10 mm in diameter) at a rotational speed of 160 rpm. Stearic acid was used as a process control agent to reduce agglomeration and decrease the cold welding effect between the particulates. The mechanical milling process was interrupted for 30 minutes after every 45 minutes of the working process to reduce excessive temperature induced

by friction between the steel powders, reinforcement (nano-ZrO_2) particles, steel balls, and steel jars.

Following the mechanical milling process, the mechanically milled particulates were pressed at room temperature under a pressure of 1000 MPa. In austenitic stainless steels, low stacking fault energy (SFE) can induce the TRIP effect, which improves the mechanical properties. SFE diminishes as the amount of plastic deformation increases and the temperature decreases during the deformation process. Because of the low temperature of the process, the cold pressing method was used, and the applied pressure was as high as possible to provide a considerable degree of plastic deformation in the mechanically milled particulates. Finally, the pressed particulates were sintered in a tube furnace at a heating rate of 5 min/ºC at 1280 ºC super-solidus temperature for 2 hours under an argon atmosphere.

The physical and mechanical properties of Cr-Ni steel and Cr-Ni/ZrO_2 nanocomposites were determined using density measurement, hardness, and compression tests. The experimental density of the specimens was measured using Archimedes' principle in accordance with ASTM B962-17. The theoretical density of the specimens was calculated using the Rule of Mixtures (ROM). The relative density of the specimens was determined by comparing (proportioning) their experimental and theoretical densities. Porosity in the specimens was calculated using the following formula: Porosity = [1 − (experimental density/theoretical density)] × 100% (Shyn *et al*. 2021).

Brinell hardness testing (Mitutoyo HR-530) was performed for 15 seconds at 187.5 kgf using a hardened steel ball with a diameter of 2.5 mm in accordance with ASTM E10-15. According to ASTM E9, cylindrical specimens with a diameter of 25 mm and a length of 75 mm were manufactured for the compression test. The compression test was performed by a testing machine (Shimadzu EHF-EV200k2-040-0A) with a load cell of 200 kN and a strain rate of 0.005 min^{-1}.

The microstructural properties of the specimens were characterized by using Scanning Electron Microscopy (SEM) (Thermo Scientific Apreo S and Zeiss 300VP) with Energy Dispersive X-Ray (EDX) detector. X-Ray Diffraction (XRD, Rigaku Ultima-IV using Cu Kα radiation (λ = 1.5406 Å)) was conducted for qualitative phase analysis.

Some methods, such as Scherrer and Williamson-Hall, are used to determine the crystallite size of materials using XRD analysis. The Scherrer equation assumes that the X-ray peak broadening is solely determined by crystallite size (Scherrer 1918). The Williamson-Hall method, on the other hand, considers not only the crystallite size but also the lattice strain of the material. Among the crystallite size calculation methods, the Williamson-Hall method is the most accurate and offers critical material properties such as structural parameters and strain (Kibasomba *et al*. 2018). Therefore, in this study, the crystallite sizes of Cr-Ni steel and Cr-Ni/ZrO_2 nanocomposites were determined using the Williamson-Hall equation (Williamson and Hall 1953) as follows:

$$\beta_{hkl}\, cos\theta = \frac{K\,\lambda}{D} + 4\,\varepsilon\, sin\theta \quad (1)$$

where β is the line broadening at half the maximum intensity (FWHM), θ is the Bragg angle, λ is the wavelength of X-ray radiation (Cu K-α, 1.5406), D is the crystallite size, ε is the lattice strain, and K is a constant and its value is assumed to be 0.94 (Shashanka and Debasis 2017).

3. Results and discussion

3.1 Microstructural properties

Figs. 2 and 3 show mechanically milled Cr-Ni steel and Cr-Ni-steel/ZrO_2 particulates. The high-energy ball milling (mechanical milling) process has a considerable impact on the shape and hardness of the particulates, as well as the distribution of the reinforcement particles in the matrix powders. The properties of mechanically milled particulates influence their densification and plastic deformation behaviors during subsequent processes such as pressing. Three primary mechanisms occur during the mechanical milling process: plastic deformation, cold-welding, and particulate fragmentation. These mechanisms arise as a result of the balls transmitting their energy to the particulates (powders) due to rotational movement during the mechanical milling process. Plastic deformation and cold-welding of powders are the major mechanisms in the initial (early) stage of the process. Because of the high plastic deformation of the powders at this stage, their shape changes from sphere to flake as seen in Fig. 2(a). As the milling process continues, the powders become larger-sized thinner layers (flakes) due to severe plastic deformation, and then these flakes begin to bond with one another by cold-welding (Fig. 2(b)), which creates particulates (Suryanarayana 2019). Particulates begin to fragment (fracture) into smaller ones at the next stage of the process (Fig. 2(c)), and then a steady-state equilibrium is attained when the rate of cold-welding is balanced by the rate of fragmentation. Particulates become smaller and smaller due to fragmentation at this stage because they have undergone strain hardening and have become more brittle. As seen in Fig. 3(a), at the end of the mechanical milling process, Cr-Ni powders underwent plastic deformation and their shape changed from spherical to flake, while cold welding occurred in some of them. While cold welding and fragmentation occurred in Cr-Ni/ZrO_2 particulates with relatively low nanoparticle ratios, fragmentation became the dominant mechanism as the nanoparticle ratio increased, resulting in smaller particulate sizes (Figs. 3(b)-(f)). The formation of smaller and equiaxial Cr-Ni/ZrO_2 particulates indicates that the nano-ZrO_2 reinforcement particles were effective at accelerating the milling process to reach the steady-state regime. Similar behavior has been observed in studies investigating the effects of reinforcement particles and their ratios (amounts) on the size of mechanically milled particulates (Kamrani *et al*. 2009, Saheb *et al*. 2015, Cabeza *et al*. 2017). This behavior can be explained as follows: Hard reinforcement particles generate a stress concentration effect in the surrounding matrix (in the vicinity of the reinforcement particle), resulting in additional deformation hardening in these regions. The high strain hardening of the particulates leads them to fracture in

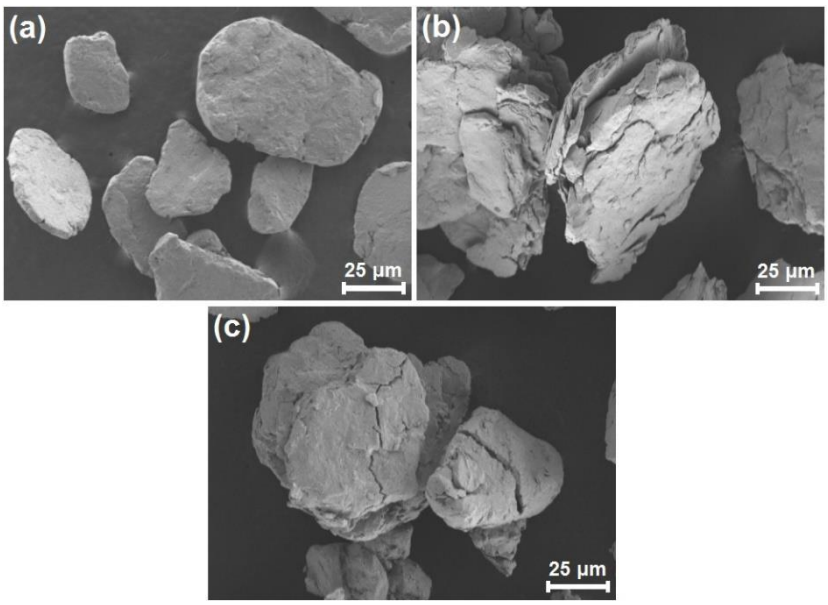

Fig. 2 SEM images of (a) plastically deformed, (b) cold-welded, and (c) fragmented particulates formed during the high-energy ball milling process

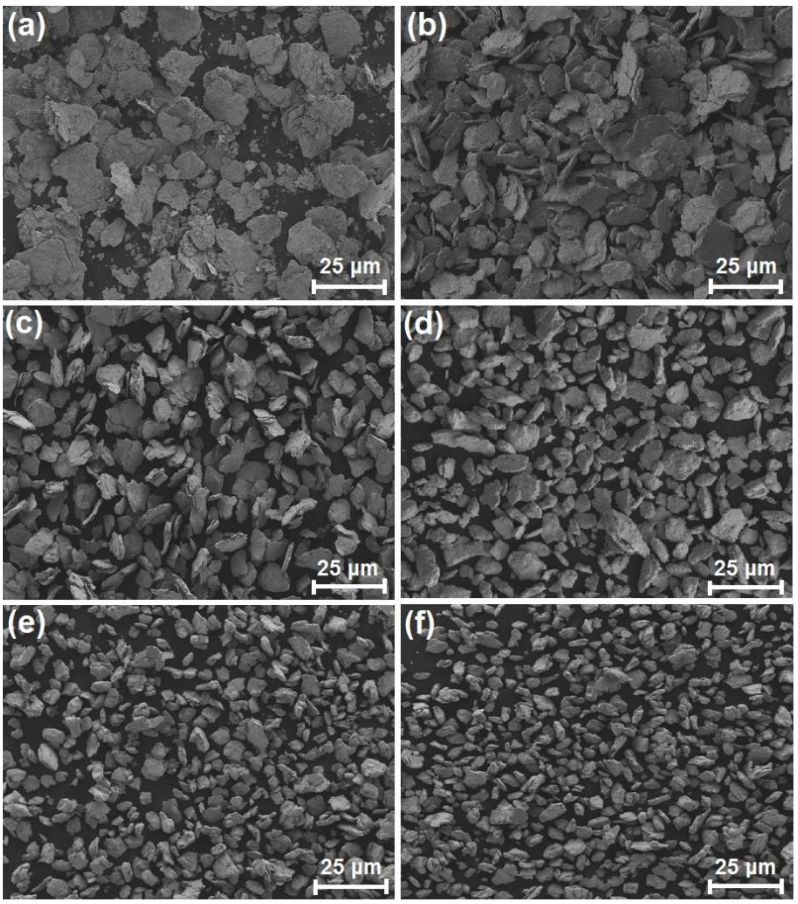

Fig. 3 SEM images of the mechanically milled (a) Cr-Ni, (b) Cr-Ni/ZrO_2 (1 wt.%), (c) Cr-Ni/ZrO_2 (2 wt.%), (d) Cr-Ni/ZrO_2 (3 wt.%), (e) Cr-Ni/ZrO_2 (4 wt.%), and (f) Cr-Ni/ZrO_2 (5wt.%) particulates

a shorter milling time, resulting in a reduction in their size (Cabeza *et al*. 2017). Therefore, in this study, nano-ZrO_2 particles were effective in reducing the size of mechanically milled Cr-Ni/ZrO_2 particulates, and their effectiveness increased, as the weight fraction of nano-ZrO_2 particles rose.

The effect of the reinforcement particles on particulate size reduction contributes to improving the mechanical

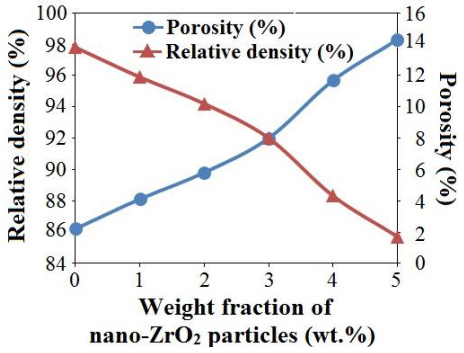

Fig. 4 Relative densities and porosities of Cr-Ni steel and CrNi/ZrO_2 nanocomposites

properties of particle-reinforced composites (Abu-Qqail *et al*. 2019). Because the interaction of dislocation/ nano-particles and the number of dislocations are higher due to Orowan theory, the nanoparticles have a greater influence on the reduction of the grain size in particulates than the microparticles (Saberi *et al*. 2009). Therefore, grain refinement due to the presence of nanoparticles during the mechanical milling process may have contributed to the improvement of the mechanical characteristics of the Cr-Ni/ZrO_2 nanocomposites.

During the mechanical milling process, hard ceramic particles in a particulate increase the deformation of the matrix surrounding these hard particles, enhancing the strain (work) hardening of the particulate matrix (Abu-Qqail *et al*. 2019). As a result, particulate produced by the mechanical milling of ceramic particles and metal powders has a higher hardness than particulate formed only of metal powders. Unfortunately, this may cause the compressibility (deformation) of mechanically milled particulates to decrease during the pressing (compaction) process used to densify the particulates after the mechanical milling process. The reduced compressibility of particulates makes it difficult to close the voids (pores) between them. It should also be noted that nanoparticles agglomerate more easily than microparticles (Liu *et al*. 2018) because of the fact that they have higher surface energy due to their higher surface area to volume ratio and agglomerate (cluster) among themselves to reduce their surface energy. For all of these reasons, the densification of particulates becomes more difficult as the amount of nanoparticles increases. In this study, as the weight fraction of nanoparticles increased, the number of pores in Cr-Ni/ZrO_2 nanocomposites may have increased for these reasons (Fig. 4).

When the process temperature surpasses the solid-state temperature of steel, undesirable reaction products such as carbide precipitates can form at the grain boundaries of the steel (Srisuwan *et al*. 2016). Although the amount of carbon in steel powders was low for the formation of carbide precipitates prior to the manufacturing processes in this study (Table 1), chrome carbide precipitates were observed in unreinforced Cr-Ni steel and Cr-Ni/ZrO_2 nanocomposites (Fig. 5), as detected by EDX and XRD analyses (Figs. 6 and 7). The carbon required for the formation of chromium carbide precipitates may have come from the wear of the steel milling jars and balls, and the stearic acid used as a process control agent in the mechanical milling process. Furthermore, the high temperature in the sintering process may have induced carbide precipitation. As seen in Fig. 5, the amount of carbide precipitates decreased as the weight fraction of nano-ZrO_2 particles increased. When reinforcement particles locate in the grain boundary, they cause a discontinuity and occupy some parts (regions) of the grain boundary. This causes an impediment to chromium diffusion to the grain boundary; therefore, chromium can diffuse into the rest (remaining) regions of the grain boundary and interacts with carbon to form chromium carbide precipitates. For this reason, the number of carbide precipitates in Cr-Ni/ZrO_2 nanocomposites in this study may have been lower than in unreinforced Cr-Ni steel and may have been reduced as the weight fraction of nano-ZrO_2 particles increased.

Stacking fault energy (SFE) affects martensitic phase transformations and mechanical twinning in austenitic stainless steels (Pierce *et al*. 2015, Galindo-Nava and Rivera-Diaz-del-Castillo 2017, Kim *et al*. 2020, Woo *et al*. 2020). SFE of steels containing Cr and Ni alloying elements can be calculated using various equations derived from linear regression of several experimental SFE data obtained from the relevant studies in the literature (Schramm and Reed 1975, Brofman and Ansell 1978, Li *et al*. 1999). The experimental SFE values can be determined using a variety of methods, including X-ray diffraction (XRD) (Kumar *et al*. 2019), transmission electron microscopy (TEM) (Lu *et al*. 2016), thermodynamics (Wang and Xiong, 2020), and the embedded-atom method (EAM) (Zhou *et al*. 2018). These methods use a variety of parameters such as the lattice parameter, microstrain, and the area occupied by one atom. Because of the large number of factors and the wide range of these factor values, various equations have been developed to calculate the SFE values of Cr-Ni steels. It should also be noted that in the experimental studies used to develop these equations, the ratios of Cr and Ni alloying elements varied and ranged widely. Because of these reasons, the SFE of Cr-Ni steel was calculated in this study using various formulas rather than a single formula (equation) (Table 2). According to the equations of Brofman and Ansell (1978) and Li *et al*. (1999), SFE values of Cr-Ni steel were calculated as 16.33 and 15.91, respectively (Table 2), which indicates that the Cr-Ni steel could be TRIP steel because SFE was less than the value of 20 mJ/m^2. It could, however, be a TWIP steel because its value was calculated to be higher than 20 mJ/m^2 according to the equations of Schramm and Reed (1975) (Table 2). It should be noted that the TWIP effect is observed in Cr-Mn-Ni steels with a high manganese concentration (Mn) (Weidner and Biermann 2015, Opiela *et al*. 2020). In this study, the amount of Mn in Cr-Ni steel was substantially lower in order for the TWIP mechanism to occur (Table 1). Also, although twinning was observed in the microstructures Cr-Ni/ZrO_2 nanocomposites (Fig. 8), which indicates the TWIP effect, few twinning occurred. For all of these reasons, it can be suggested that the TWIP mechanism is not sufficiently effective in Cr-Ni/ZrO_2 nanocomposites.

α′–martensite can be produced through dislocation movement and the generation and intersection of deformation bands (Berahmand *et al*. 2021). Ceramic

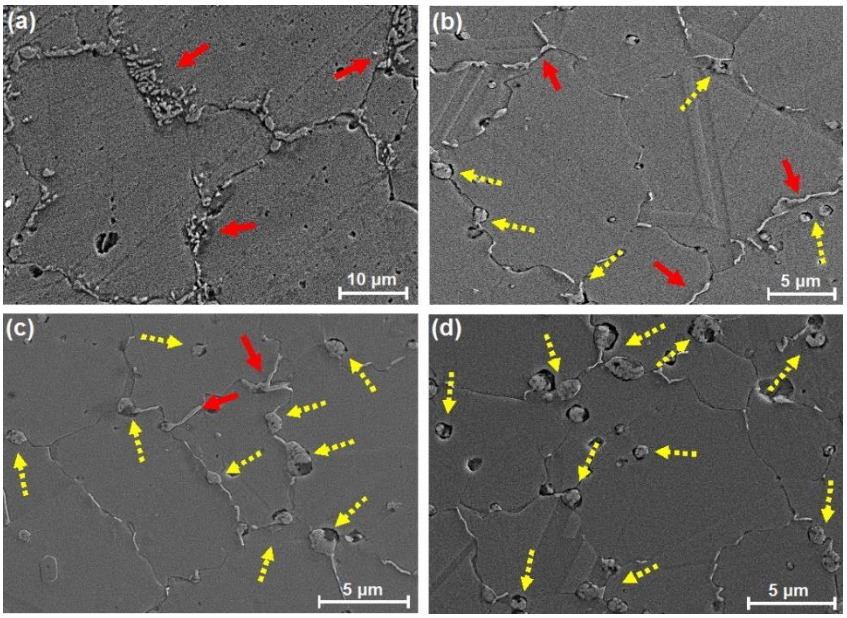

Fig. 5 SEM images of the microstructures of (a) Cr-Ni steel and (b) Cr-Ni/ZrO_2 (1 wt.%), (b) Cr-Ni/ZrO_2 (3 wt.%), (b) Cr-Ni/ZrO_2 (5 wt.%) nanocomposites (solid and dashed arrows show nano-ZrO_2 particle cluster and chromium-carbide precipitate, respectively)

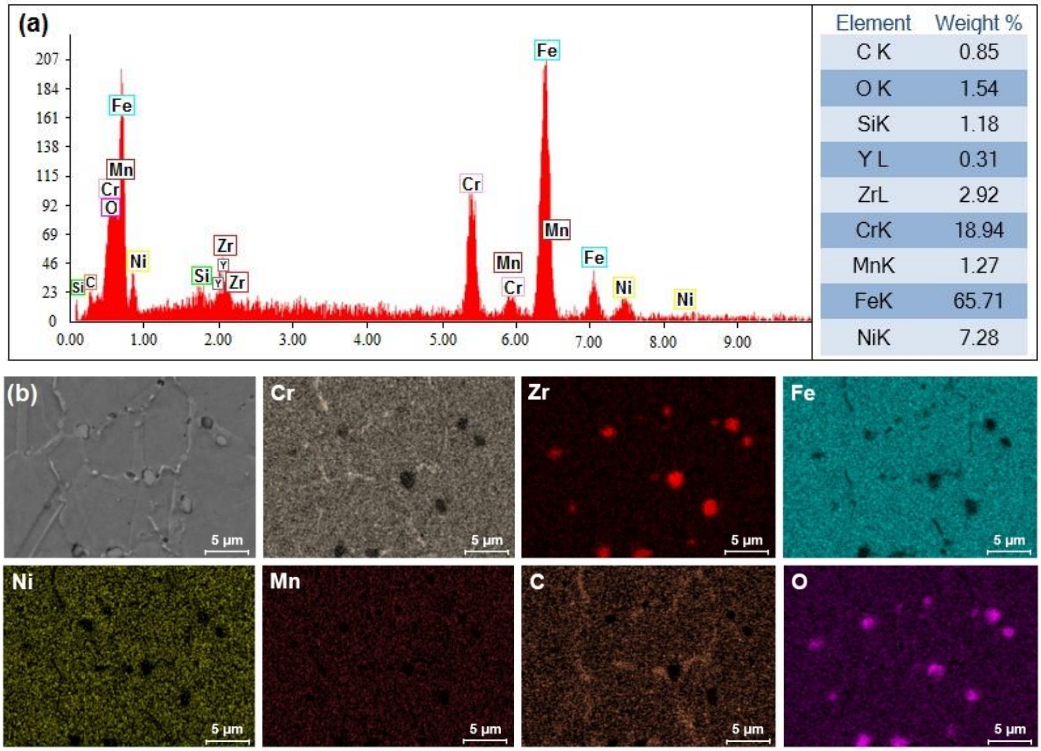

Fig. 6 EDX (a) elemental and (b) mapping analyses of Cr-Ni/ZrO_2 nanocomposite reinforced with 3 wt.% nano-ZrO_2 particles

Table 2 Formulas for the calculation of stacking fault energy (SFE) of Cr-Ni steel

Formula	SFE (mJ/m^2)
4 + 1.8 (Ni wt.%) − 0.2 (Cr wt.%) + 410 (C wt.%) (Schramm and Reed 1975)	25.51
16.7 + 2.1 (Ni wt.%) − 0.9 (Cr wt.%) + 26 (C wt.%) (Brofman and Ansell 1978)	16.33
34 + 2.4 (Ni wt.%) − 1.2 (Cr wt.%) − 1.2 (Mn wt.%) (Schramm and Reed 1975)	28.17
28.87 + 1.64 (Ni wt.%) − 1.1 (Cr wt.%) − 0.21 (Mn wt.%) − 4.45 (Si wt.%) (Li *et al*. 1999)	15.91

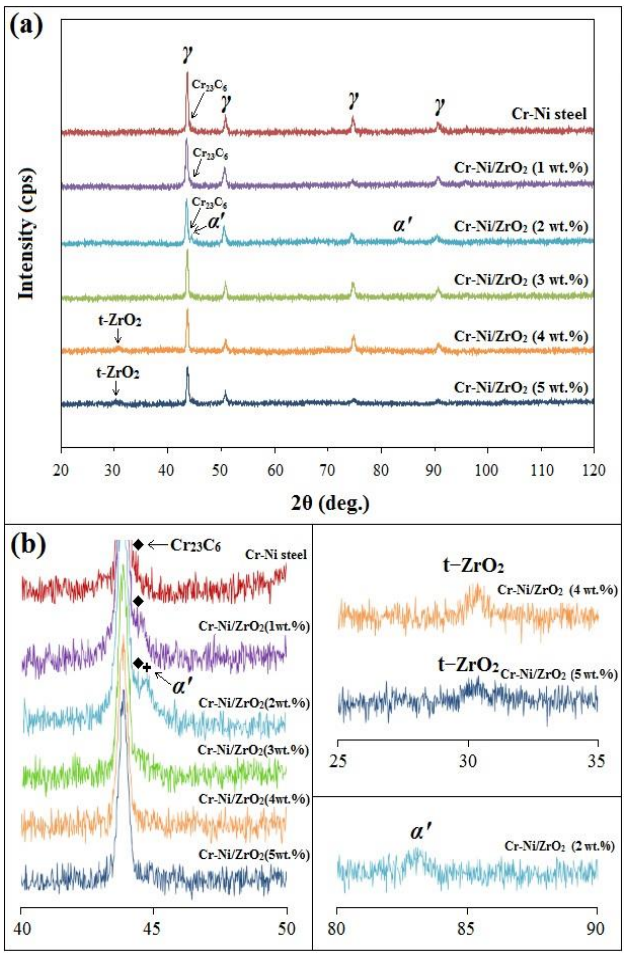

Fig. 7 XRD analyses of (a) Cr-Ni steel and Cr-Ni/ZrO_2 nanocomposites and (b) details of peaks identifying $Cr_{23}C_6$, α′, and t−ZrO_2 phases

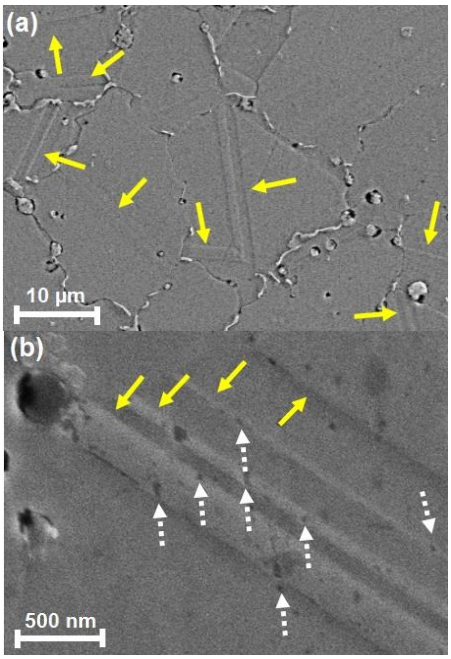

Fig. 8 SEM images of the microstructures of Cr-Ni/ZrO_2 nanocomposites: (a) deformation bands showed by solid arrows and (b) deformation bands and α′-martensite showed by solid and dashed arrows, respectively

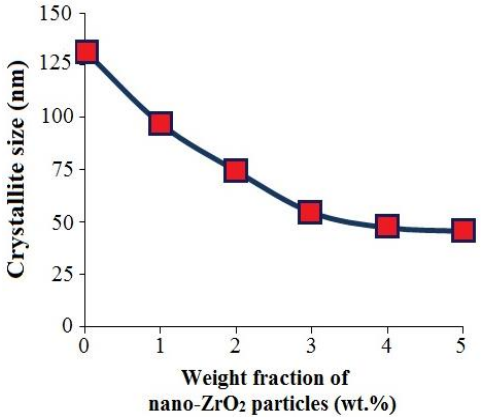

Fig. 9 Crystallite sizes of Cr-Ni steel and Cr-Ni-steel/ZrO_2 nanocomposites

reinforcement particles, such as ZrO_2 particles, may play an active role in α′–martensite formation in particle-reinforced TRIP/TWIP steel matrix composites. The load applied during mechanical milling and cold pressing can cause substantial plastic strain in the matrix surrounding the reinforcement particles. This promotes the creation of deformation bands and their intersection, resulting in the formation of α′–martensite (Martin *et al*. 2011, Prüger *et al*. 2013). Nano reinforcement particles bear more load than micro-particles. Therefore, less plastic stress occurs in the matrix surrounding the nanoparticles. Reinforcement particles can also impede the nucleation and propagation of deformation twinning (Garcés *et al*. 2016), leading to fewer and shorter deformation bands. All of these factors have a negative impact on the formation of martensite. Because of these reasons, the nano-ZrO_2 particles may have caused in low amounts of deformation bands and α′–martensite formation in the Cr-Ni/ZrO_2 nanocomposites, as seen in Fig. 8.

During the plastic deformation of TRIP steels having ZrO_2 particles, the crystalline structure of ZrO_2 particles transforms from tetragonal (t) to monoclinic (m) (Martin *et al*. 2013, Weigelt *et al*. 2015). The transformation of t–ZrO_2 → m–ZrO_2 is driven by high stress in ZrO_2 particles. In particle-reinforced composites, the stress in micro-sized reinforcement particles is higher than that in smaller ones (Sugimura and Suresh 1992). Therefore, it can be suggested that the number of phase transformations in nano-ZrO_2 particles will be lower than that in micro-ZrO_2 particles. It should also be noted that, due to thermodynamic stability, small-sized ZrO_2 particles are more stable for t–ZrO_2 → m–ZrO_2 transformation than bigger ones (Green *et al*. 2018). The transformation from t–ZrO_2 to m–ZrO_2 did not occur in this study due to these reasons. However, t–ZrO_2 was detected in Cr-Ni/ZrO_2 nanocomposites having 4 and 5 wt.% nano-ZrO_2 particles.

Phase transformations in particle-reinforced TRIP/TWIP steels result from high stress and/or efficient stress transfer between the matrix and the reinforcement particles. Particle agglomerates (clusters) in composites have a negative effect on phase transformations because stress cannot be efficiently transferred between the matrix and the particle and also the stress in and around the particle aggregates is

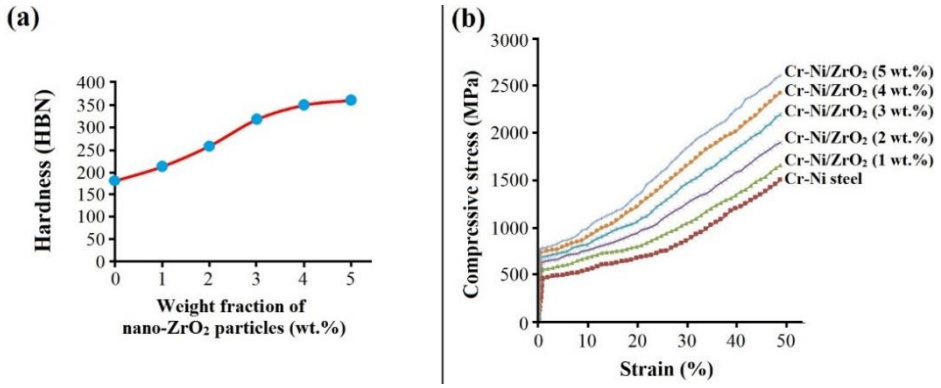

Fig. 10 (a) Hardness and (b) compressive stress-strain of Cr-Ni steel and Cr-Ni/ZrO_2 nanocomposites

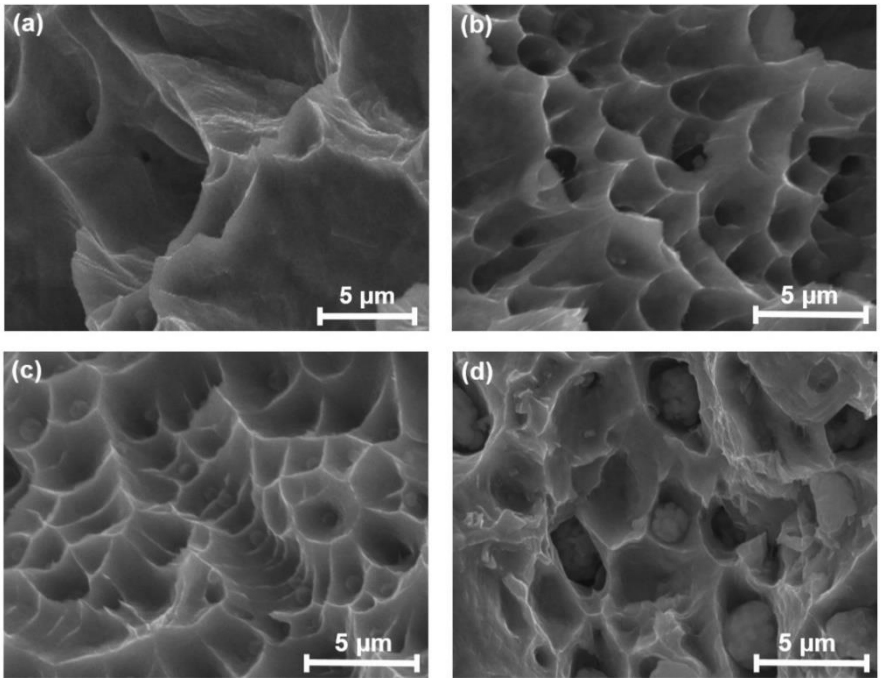

Fig. 11 SEM images of the fracture surfaces of (a) Cr-Ni steel and (b) Cr-Ni/ZrO_2 (1 wt.%), (c) Cr-Ni/ZrO_2 (2 wt.%), and (d) Cr-Ni/ZrO_2 (4 wt.%) nanocomposites

low. The number of particle aggregates rises as the number of reinforcement particles increases and their size decreases. For all of these reasons, it can be concluded in this study that nano-sized ZrO_2 particles were not sufficiently effective in the phase transformations in both the Cr-Ni steel matrix and themselves.

The crystallite sizes of Cr-Ni steel and Cr-Ni/ZrO_2 nanocomposites were calculated from XRD (Fig. 7) using Eq. (1). Due to the presence of nanoparticles and the high-energy ball milling process, the crystallite size of all Cr-Ni/ZrO_2 nanocomposites was smaller than that of Cr-Ni steel and decreased as the number (wt.%) of nanoparticles increased (Fig. 9).

3.2 Mechanical properties

Cr-Ni/ZrO_2 nanocomposite had higher hardness and compressive strength than Cr-Ni-steel, and its mechanical properties improved further as the weight fraction of nano-ZrO_2 particles increased as seen in Fig. 10. Cr-Ni/ZrO_2 nanocomposite reinforced with 5 wt% nano-ZrO_2 particles had almost twofold the hardness of Cr-Ni steel (Fig. 10(a)). This can be attributed to the hard nano-ZrO_2 particles (Madhukar *et al.* 2022) and their effect on grain (or crystallite) size reduction (Salur 2022). Nanoparticles in grain boundaries have a Zener-pinning effect (Liu *et al.* 2021), promoting the formation of a small grain microstructure by inhibiting grain growth. Fine-grained microstructures have more dislocations and more barriers to impede the movement of dislocations, leading to an increase in hardness. Therefore, as the number of nanoparticles increases, the size of the grain (or crystallite) reduces (Xu et *al.* 2017, Wu *et al.* 2020, Alam *et al.* 2022), and the hardness increases. As shown in Fig. 10, the hardness of Cr-Ni/ZrO_2 nanocomposite was higher than Cr-Ni steel and increased as the weight fraction of nano-ZrO_2 particles increased due to the reduction of crystallite size (Fig. 9).

Despite the fact that the Cr-Ni steel matrix had a low amount of phase transformations and almost no tetragonal → monoclinic transformation in the nano-ZrO_2 particles (Fig. 7), the compressive strength of Cr-Ni/ZrO_2 nanocomposites was significantly higher than that of Cr-Ni steel (Fig. 10(b)). It is an unexpected result because the phase transformations induced by the TRIP effect can yield gains in strength in austenitic steels (Lehnert *et al*. 2019, Qayyum *et al*. 2020). As a result of these findings, it can be concluded that nano-ZrO_2 particles have a considerably greater influence on particle-strengthening mechanisms than deformation-induced strengthening mechanisms on the improvement of the mechanical properties of Cr-Ni/ZrO_2 nanocomposite.

Dimples formed on the fracture surfaces indicate that Cr-Ni steel and Cr-Ni/ZrO_2 nanocomposites had ductile fracture behavior (Fig. 11). In comparison to Cr-Ni steel (Fig. 11(a)), more and smaller dimples were formed in Cr-Ni/ZrO_2 nanocomposites (Figs. 11(b)-(d)). The size of the dimples in Cr-Ni/ZrO_2 (2 wt.%) nanocomposite (Fig. 11(c)) was smaller than Cr-Ni/ZrO_2 (1 wt.%) nanocomposite (Fig. 11(b)). This can be attributed to grain refinement caused by the presence of nanoparticles and an increase in the amount of nanoparticles in nanocomposites (Mu *et al*. 2022). However, due to the high agglomeration tendency of nanoparticles, the number and size of particle aggregates increase as the amount of nanoparticles rises. At high nanoparticle ratios, the particle aggregates (clusters) grow in size and become difficult to break up (to separate agglomerated nanoparticles from each other in a particle aggregate) using the mechanical milling process. For this reason, the size of dimples formed on the fracture surface of Cr-Ni/ZrO_2 (4 wt.%) nanocomposite (Fig. 11(d)) was larger than that of Cr-Ni/ZrO_2 (2 wt.%) nanocomposite (Fig. 11(c)) although Cr-Ni/ZrO_2 (4 wt.%) nanocomposite had a smaller crystallite size (Fig. 9).

4. Conclusions

Cr-Ni/ZrO_2 nanocomposites were produced using a combination of high-energy ball milling, pressing, and sintering processes, and their microstructure and mechanical properties were investigated. Nano-ZrO_2 particles had a significant influence in reducing the crystallite size of the Cr-Ni steel and inhibiting chromium carbide precipitation at grain boundaries. The transformation from t–ZrO_2 to m–ZrO_2 was not detected. Few α'–martensite and deformation bands were formed in the microstructures of Cr-Ni/ZrO_2 nanocomposites. Nano-ZrO_2 particles were not sufficiently effective in the phase transformations in both Cr-Ni steel matrix and themselves. Therefore, they did not efficiently activate deformation-induced strengthening mechanisms. However, the mechanical properties of Cr-Ni steel were improved by reinforcing with nano-sized ZrO_2 particles. Cr-Ni-steel/ZrO_2 nanocomposite had higher hardness and compressive strength than Cr-Ni steel, and its mechanical properties improved further as the weight fraction of nano-ZrO_2 particles increased. High strain values were obtained for Cr-Ni/ZrO_2 nanocomposites, and many dimples formed on their fracture surfaces, implying that they retained the ductility of Cr-Ni steel while having higher hardness and compressive strength.

In conclusion, the nano-ZrO_2 particles were considerably more effective in particle-strengthening mechanisms than deformation-induced strengthening mechanisms and significantly improved the mechanical properties of the Cr-Ni/ZrO_2 composite.

References

Abu-Qqail, A. Wagih, A. Fathy, A.O. Elkady, Q.A. and Kabeel A.M. (2019), "Effect of high energy ball milling on strengthening of Cu-ZrO_2 nanocomposites", *Ceram. Int*., **45**(5), 5866-5875. https://doi.org/10.1016/j.ceramint.2018.12.053.

Alam, M.A. Ya, H.H. Azeem, M. Yusuf, M. Soomro, I.A. Masood, F. Shozib, I.A. Sapuan, S.M. and Akhter, J. (2022), "Artificial neural network modeling to predict the effect of milling time and TiC content on the crystallite size and lattice strain of Al7075-TiC composites fabricated by powder metallurgy", *Crystals*, **12**(3), 1-20. https://doi.org/10.3390/cryst12030372.

Berahmand, M. Ketabchi, M. Jamshidian, M. and Tsurekawa, S. (2021), "Investigation of microstructure evolution and martensite transformation developed in austenitic stainless steel subjected to a plastic strain gradient: A combination study of Mirco-XRD, EBSD, and ECCI techniques", *Micron*, **143**(103014), 1-12. https://doi.org/10.1016/j.micron.2021.103014.

Berek, H. Yanina, A. Weigelt, C. and Aneziris, C.G. (2011), "Determination of the phase distribution in sintered TRIP-matrix/Mg-PSZ composites using EBSD", *Steel Res. Int*., **82**(9), 1094-1100. https://doi.org/10.1002/srin.201100064.

Bhoi, N.K. Singh, H. and Pratap, S. (2020), "Developments in the aluminum metal matrix composites reinforced by micro/nano particles – A review", *J. Compos. Mater*., **54**(6), 813-833. https://doi.org/10.1177/0021998319865307.

Biermann, H. and Aneziris, C.G. (2020), *Austenitic TRIP/TWIP Steels and Steels Zirconia–Composites*, Springer, Cham, Switzerland.

Brofman, P.J. and Ansell, G.S. (1978), "On the effect of carbon on the stacking fault energy of austenitic stainless steels", *Metall. Mater. Trans. A*, **9**, 879-880. https://doi.org/10.1007/BF02649799.

Casati, R. and Vedani, M. (2014), "Metal matrix composites reinforced by nano-particles – A review", *Metals*, **4**(1), 65-83. https://doi.org/10.3390/met4010065.

Cabeza, M. Feijoo, I. Merino, P. Pena, G. Pérez, M.C. Cruz, S. and Rey, P. (2017), "Effect of high energy ball milling on the morphology, microstructure and properties of nano-sized TiC particle-reinforced 6005A aluminium alloy matrix composite", *Powder Technol*., **321**, 31-43. https://doi.org/10.1016/j.powtec.2017.07.089.

Eckner, R. Krampf, M. Segel, C. and Krüger L. (2016), "Strength and fracture behavior of a particle-reinforced transformation-toughened trip steel/ZrO_2 composite", *Mech. Compos. Mater*., **51**, 707-720. https://doi.org/10.1007/s11029-016-9541-z.

El-Sherbiny, A. El-Fawkhry, M.K. Shash, A.Y. and Hossany T.E. (2020), "Replacement of silicon by aluminum with the aid of vanadium for galvanized TRIP steel", *J. Mater. Res. Technol*. **9**(3), 3578-3589. https://doi.org/10.1016/j.jmrt.2020.01.096.

Galindo-Nava, E.I. and Rivera-Diaz-del-Castillo, P. E. J. (2017), "Understanding martensite and twin formation in austenite steels: A model describing TRIP and TWIN effects", *Acta Mater*., **128**, 120-134.

https://doi.org/10.1016/j.actamat.2017.02.004.
Garcés, G. Máthis, K. Pérez, P. Čapek, J. and Adeva, P., (2016), "Effect of reinforcing shape on twinning in extruded magnesium matrix composites", *Mater. Sci. Eng. A.*, **666**, 48-53. https://doi.org/10.1016/j.msea.2016.04.028.
Glage, A. Weigelt, C. Rathel, J. and Biermann H. (2013), "Influence of matrix strength and volume fraction of Mg-PSZ on the cyclic deformation behavior of hot pressed TRIP/TWIP-matrix composite materials", *Adv. Eng. Mater.*, **15**(7), 550-557. https://doi.org/10.1002/adem.201200334.
Green, D.J., Hannink, R.H.J. and Swain, M.V. (2018), *Transformation Toughening of Ceramics*, CRC Press, Boca Raton, Florida, U.S.A.
Järvenpää, A. Jaskari, M. Kisko, A. and Karjalainen, P. (2020), "Processing and properties of reversion-treated austenitic stainless steels", *Metals*, **10**(281), 1-43. https://doi.org/10.3390/met10020281.
Kamrani, S. Riedel, R. Seyed Reihani S.M. and Kleebe, H.J. (2009), "Effect of reinforcement volume fraction on the mechanical properties of Al—SiC nanocomposites produced by mechanical alloying and consolidation", *J. Compos. Mater.*, **44**(3), 313-326. https://doi.org/10.1177/0021998309347570.
Kibasomba, P.M. Dhlamini, S. Maaza, Liu, C.P. Rashad, M.M. Rayan, D.A. and Mwakikunga, B.W. (2018), "Strain and grain size of TiO_2 nanoparticles from TEM, Raman spectroscopy and XRD: The revisiting of the Williamson-Hall plot method", *Results Phys.*, **9**, 628-635. https://doi.org/10.1016/j.rinp.2018.03.008.
Kim, Y. Choi, W. Choo, H. An, K. Choi, H.S. and Lee, S.Y. (2020), "In situ neutron diffraction study of phase transformation of high Mn steel with different carbon content", *Crystals*, **10**(101), 1-13. https://doi.org/10.3390/cryst10020101.
Kirschner, M. Guk, S. Kawalla, R. and Prahl, U. (2021), "Powder forging of in axial and radial direction graded components of TRIP-matrix-composite", *Metals*, **11**(3), 1-17. https://doi.org/10.3390/met11030378
Kumar, S. Samantaraya, D. Aashranth, B. Keskar, N. Davinci, M.A. Borah, U. Srivastava, D. and Bhaduri, A.K. (2019), "Dependency of rate sensitive DRX behaviour on interstitial content of a FeCr-Ni-Mo alloy", *Mater. Sci. Eng. A.*, **743**, 148-158. https://doi.org/10.1016/j.msea.2018.11.062.
Lehnert, R. Weidner, A. Motylenko, M. and Biermann H. (2019), "Strain hardening of phases in high-alloy CrMnNi steel as a consequence of pre-deformation studied by nanoindentation", *Adv. Eng. Mater.*, **21**(5)1800801, 1-14. https://doi.org/10.1002/adem.201800801.
Li, J. Zheng, W. and Jiang, Q. (1999), "Stacking fault energy of iron-based shape memory alloys", *Mater. Lett.*, **38**(4), 275-277. https://doi.org/10.1016/S0167-577X(98)00172-4.
Liu, J. Chen, Z. Zhang, F. Ji, G. Wang, M. Ma, Y. Ji, V. Zhong S. Wu, Y. and Wang, H. (2018), "Simultaneously increasing strength and ductility of nanoparticles reinforced Al composites via accumulative orthogonal extrusion process", *Mater. Res. Lett.*, **6**(8), 406-412. https://doi.org/10.1080/21663831.2018.1471421.
Liu, J. Zhang, Q. Chen, Z. Wang, L. Ji, G. Shi, Q. Wu, Y. Zhang, F. and Wang, H. (2021), "Fabrication of fine grain structures in Al matrices at elevated temperature by the stimulation of dual-size particles", *Mater. Sci. Eng. A.*, **805**(140614), 1-10. https://doi.org/10.1016/j.msea.2020.140614.
Lu, J. Hultman, L. Holmström, E. Antonsson, K.H. Grehk, M. Li, W. Vitos, L. and Golpayegani, A. (2016), "Stacking fault energies in austenitic stainless steels", *Acta Mater.*, **111**, 39-46. https://doi.org/10.1016/j.actamat.2016.03.042.
Madhukar, P. Selvaraj, N. Kumar, G.B.V. Rao, C.S.B. Mohammad, F. Seetharam, R. and Chaval, M. (2022), "Influence of TiC nano-particulates on the physical andmechanical properties of AA7150-TiC MMC: Fabricated by advanced novel process", *Nano Select*, **3**(1), 78-90. https://doi.org/10.1002/nano.202100094.
Malaki, M. Xu, W. Kasar, A.K. Menezes, P.L. Dieringa, H. Varma, R.S. and Gupta, M. (2019), "Advanced metal matrix composites", *Metals*, **9**(3), 330, 1-39. https://doi.org/10.3390/met9030330.
Martin, S. Richter, S. Decker, S. Martin, U. Krüger, L. and Rafaja, D. (2011), "Reinforcing mechanism of Mg-PSZ particles in highly-alloyed TRIP steel", *Steel Res. Int.*, **82**(9), 1133-1140. https://doi.org/10.1002/srin.201100099.
Martin, S. Richter, S. Poklad, A. Berek, H. Decker, S. Martin, U. Krüger, L. and Rafaja D. (2013), "Orientation relationships between phases arising during compression testing in ZrO_2-TRIP-steel composite", *J. Alloys. Compd.*, **577**, S578-S582. https://doi.org/10.1016/j.jallcom.2012.02.014.
Mu, D. Zhang, Z. Liang, J. Wang, J. and Zhang, D. (2022), "Investigation of microstructures and mechanical properties of SiC/AA2024 nanocomposites processed by powder metallurgy and T6 heat treatment", *Materials*, **15**(3547), 1-16. https://doi.org/10.3390/ma15103547.
Opiela, M. Fojt-Dymara, G. Grajcar, A. and Borek, W. (2020), "Effect of grain size on the microstructure and strain hardening behavior of solution heat-treated low-C high-Mn steel", *Materials*, **13**(1489), 1-13. https://doi.org/10.3390/ma13071489.
Pierce, D.T. Jimenez, J.A. Bentley, J. Raabe, D. and Wittig, J.E. (2015), "The influence of stacking fault energy on the microstructural and strain-hardening evolution of Fe-Mn-Al-Si steels during tensile deformation", *Acta Mater.*, **100**, 178-190. https://doi.org/10.1016/j.actamat.2015.08.030.
Prüger, S. Mehlhorn, L. Mühlic, U. and Kuna, M. (2013), "Study of reinforcing mechanisms in TRIP-matrix composites under compressive loading by means of micromechanical simulations", *Adv. Eng. Mater.*, **15**(7), 542-549. https://doi.org/10.1002/adem.201200323.
Qayyum, F. Guk, S. Schmidtchen, M. Kawalla, R. and Prahl, R. (2020), "Modeling the local deformation and transformation behavior of cast X8CrMnNi16-6-6 TRIP steel and 10% Mg-PSZ composite using a continuum mechanics-based crystal plasticity model", *Crystals*, **10**(221), 1-25. https://doi.org/10.3390/cryst10030221.
Saberi, Y. Zebarjad, S.M. and Akbari, G.H. (2009), "On the role of nano-size SiC on the lattice strain and grain size of Al/SiC nanocomposite", *J. Alloy. Compd.*, **484**, 637-640. https://doi.org/10.1016/j.jallcom.2009.05.009.
Saheb, N. Khan, M.S. and Hakeem, A.S. (2015), "Effect of processing on mechanically alloyed and spark plasma sintered Al-Al_2O_3 nanocomposites", *J. Nanomater.*, **2015**(609824), 1-13. https://doi.org/10.1155/2015/609824.
Salur, E. (2022), "Synergistic effect of ball milling time and nano-sized Y_2O_3 addition on hardening of Cu-based nanocomposites", *Arch. Civ. Mech.*, **22**(103), 1-18. https://doi.org/10.1007/s43452-022-00429-1.
Scherrer, P. (1918), "Nachrichten von der gesellschaft der wissenschaften zu göttingen", *Math. Phys. Kl.*, **2**, 98-100.
Schramm, R.E. and Reed, R.P. (1975), "Stacking fault energies of seven commercial austenitic stainless steels", *Metall .Trans. A.*, **6A**, 1345-1351. https://doi.org/10.1007/BF02641927.
Shashanka, R. and Debasis, C. (2017), *Ball Milled Nano-Structured Stainless Steel Powders*, Educreation Publishing, New Delhi, India.
Shyn, C.S. Rajesh, R. and Anand M.D. (2021), "A6061/B4C MMCs fabrication, experimental investigation and prediction of properties", *IOP Conf. Ser.: Mater. Sci. Eng.*, **1017**(012003), 1-13. https://doi.org/10.1088/1757-899X/1017/1/012003.
Song, G.S. Ji, K.S. Song, H.W. and Zhang, S.H. (2019), "Microstructure and transformation and twinning mechanism of

304 stainless steel tube during hydraulic bulging", *Mater. Res. Express*, **6**(12), 1-12. https://doi.org/10.1088/2053-1591/ab5375.

Srisuwan, N. Eidhed, K. Kreatsereekul, N. Yingsamphanchareon, T. and Kaewvilai, A. (2016), "The study of heat treatment effects on chromium carbide precipitation of 35Cr-45Ni-Nb Alloy for repairing furnace tubes", *Metals*, **6**(1), 26. https://doi.org/10.3390/met6010026.

Sugimura, Y. and Suresh, S. (1992), "Effects of SiC content on fatigue crack growth in", *Metall. Trans. A.*, **23**, 2231-2242. https://doi.org/10.1007/BF02646016.

Suryanarayana, C. (2019), "Mechanical alloying: A novel technique to synthesize advanced materials", *Research*, **4219812**, 1-17. https://doi.org/10.34133/2019/4219812.

Wang, X. and Xiong, W. (2020), "Stacking fault energy prediction for austenitic steels: thermodynamic modeling vs. machine learning", **21**(1), 626-634. https://doi.org/10.1080/14686996.2020.1808433.

Weigelt, C. Berek, H. Aneziris, C.G. Wolf, S. Eckner, R. and Krüger, L. (2015), "Effect of minor titanium additions on the phase composition of TRIP steel/magnesia partially stabilised zirconia composite materials", *Ceram. Int.*, **41**(2), 2328-2335. https://doi.org/10.1016/j.ceramint.2014.10.040.

Weigelt, C. Schmidt, G. Anerizis, C.G. Eckner, R. Ehinger, D. Krüger, L. Ullrich, C. and Rafaja, D. (2017), "Compressive and tensile deformation behaviour of TRIP steel-matrix composite materials with reinforcing additions of zirconia and/or aluminium titanate", *J. Alloy. Compd.*, **695**, 9-20. https://doi.org/10.1016/j.jallcom.2016.10.176

Weidner, A. (2020), *Deformation Processes in TRIP/TWIN Steels: In-Situ Characterization Techniques*, Springer, Cham, Switzerland.

Weidner, A. and Biermann, H. (2015), "Combination of different in situ characterization techniques and scanning electron microscopy investigations for a comprehensive description of the tensile deformation behavior of a CrMnNi TRIP/TWIP Steel", *JOM*, **67**(8), 1729-1747. https://doi.org/10.1007/s11837-015-1456-y.

Williamson, G.K. and Hall, W.H. (1953), "X-ray line broadening from filled aluminium and wolfram", *Acta Metall.*, **1**(1), 22-31. https://doi.org/10.1016/0001-6160(53)90006-6.

Woo, W. Jeong, J.S. Kim, D.K. Lee, C.M. Choi, S.H. Suh, J.Y. Lee, S.Y. Harjo, S. and Kawasaki, T. (2020), "Steel 316L and CrCoNi medium entropy alloy using in situ neutron diffraction", *Sci. Rep.*, **10**(1350), 1-15. https://doi.org/10.1038/s41598-020-58273-3.

Wu, Q. Miao, W.S., Zhang, Y.D. Gao, H.J. and Hui, D. (2020), "Mechanical properties of nanomaterials: A review", *Nanotechnol. Rev.*, **9**(1), 259-273. https://doi.org/10.1515/ntrev-2020-0021.

Xu, W. Galano, M. and Audebert, F. (2017), "Nanoquasicrystalline Al-Fe-Cr-Ti alloy matrix/γ-Al_2O_3 nanocomposite powders: The effect of the ball milling process", *J. Alloys Compd.*, **701**, 342-349. https://doi.org/10.1016/j.jallcom.2016.11.412.

Zhao, K. Duan, Z. Liu, J. Kang, G. and An, L. (2022), "Strengthening mechanisms of 15 vol.% Al_2O_3 nanoparticles reinforced aluminum matrix nanocomposite fabricated by high energy ball milling and vacuum hot pressing", *Acta Metall. Sin.-Engl.*, **35**(6), 915-921. https://doi.org/10.1007/s40195-021-01306-1.

Zhou, X.W. Foster, M.E. Sills, and R.B. (2018), "An Fe-Ni-Cr embedded atom method potential for austenitic and ferritic systems", *J. Comput. Cam.*, **39**(29), 2420-2431. https://doi.org/10.1002/jcc.25573.